Article

Measurement of the Free-Energy Dependence of Interfacial Charge-Transfer Rate Constants using ZnO/HO Semiconductor/Liquid Contacts

Thomas W. Hamann, Florian Gstrein, Bruce S. Brunschwig, and Nathan S. Lewis

J. Am. Chem. Soc., **2005**, 127 (21), 7815-7824• DOI: 10.1021/ja0436188 • Publication Date (Web): 07 May 2005

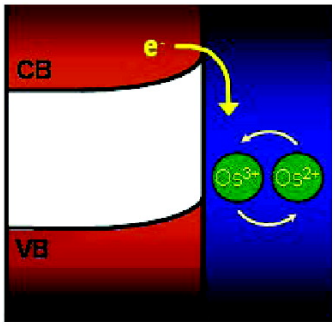

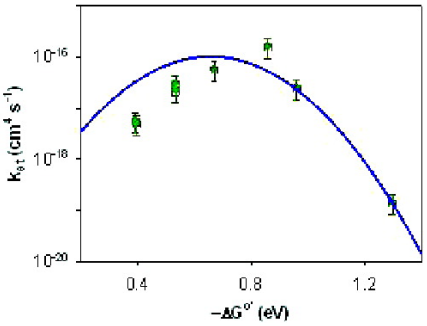

More About This Article

Additional resources and features associated with this article are available within the HTML version:

- Supporting Information
- Links to the 7 articles that cite this article, as of the time of this article download
- Access to high resolution figures
- Links to articles and content related to this article
- Copyright permission to reproduce figures and/or text from this article

View the Full Text HTML

J|A|C|S
ARTICLES
Published on Web 05/07/2005

Measurement of the Free-Energy Dependence of Interfacial Charge-Transfer Rate Constants using ZnO/H_2O Semiconductor/Liquid Contacts

Thomas W. Hamann, Florian Gstrein, Bruce S. Brunschwig, and Nathan S. Lewis*

Contribution from the Division of Chemistry and Chemical Engineering, Noyes Laboratory, 127-72, California Institute of Technology, Pasadena, California 91125

Received October 20, 2004; E-mail: nslewis@caltech.edu

Abstract: The dependence of electron-transfer rate constants on the driving force for interfacial charge transfer has been investigated using n-type ZnO electrodes in aqueous solutions. Differential capacitance versus potential and current density versus potential measurements were used to determine the energetics and kinetics, respectively, of the interfacial electron-transfer processes. A series of nonadsorbing, one-electron, outer-sphere redox couples with formal reduction potentials that spanned approximately 900 mV allowed evaluation of both the normal and Marcus inverted regions of interfacial electron-transfer processes. All rate processes were observed to be kinetically first-order in the concentration of surface electrons and first-order in the concentration of dissolved redox acceptors. The band-edge positions of the ZnO were essentially independent of the Nernstian potential of the solution over the range 0.106−1.001 V vs SCE. The rate constant at optimal exoergicity was observed to be approximately 10^{-16} cm^4 s^{-1}. The rate constant versus driving force dependence at n-type ZnO electrodes exhibited both normal and inverted regions, and the data were well-fit by a parabola generated using classical Marcus theory with a reorganization energy of 0.67 eV. NMR line broadening measurements of the self-exchange rate constants indicated that the redox couples had reorganization energies of 0.64−0.69 eV. The agreement between the reorganization energy of the ions in solution and the reorganization energy for the interfacial electron-transfer processes indicated that the reorganization energy was dominated by the redox species in the electrolyte, as expected from an application of Marcus theory to semiconductor electrodes.

I. Introduction

A. Background. The Marcus semiclassical description of outer-sphere electron-transfer reactions has been studied extensively for electron-transfer processes between molecular donor and acceptor species.[1] Agreement between theory and experiment has been demonstrated in numerous cases.[2−5] In contrast, there have been relatively few studies of electron transfer at semiconductor/liquid contacts. Current versus potential data for electron transfer from ZnO to deuterated and normal thianthrene acceptors were interpreted in terms of the normal and inverted regions of Marcus theory.[6] Transient absorption data for a series of TiO_2−$Fe(CN)_5L$ contacts that showed increasing excited-state lifetimes with increasing relative driving force were presented as evidence of the inverted region.[7]

For nonadsorbed, outer-sphere redox species, extraordinarily low defect densities at the semiconductor/liquid interface are required to prevent adsorption and surface-state-related reactions from dominating the observed interfacial kinetics processes.[8,9] Carefully prepared (100)-oriented n-type Si/CH_3OH viologen$^{2+/+}$ contacts have shown the predicted dependence of interfacial charge-transfer rate constants, k_{et}, on changes in standard interfacial free energies, $\Delta G°'$,[10] for driving forces up to, and slightly beyond, that of optimal exoergicity. However, measurements at higher driving forces were precluded because redox couples having more positive potentials than the valence band edge of Si oxidize the Si surface and/or induce carrier inversion processes that prevent changes in interfacial driving force as the Nernstian potential of the electrolyte is increased.[11] Similar considerations limit the experimentally accessible range of driving forces for InP electrodes.[12] Such considerations are expected to complicate kinetics measurements at high exoergicity for other small band gap (<2 eV) semiconducting electrodes as well.

The metal oxide semiconductor, ZnO, is an attractive material to mitigate these drawbacks and, thereby, allow direct investigation of the behavior of k_{et} at large interfacial exoergicities. The wide band gap of ZnO (3.3 eV) allows a large variation in the driving force, and ZnO is not susceptible to the oxidation or passivation processes that are prevalent in small band gap semiconductors.

(1) Marcus, R. A.; Sutin, N. *Biochim. Biophys. Acta* **1985**, *811*, 265−322.
(2) Chou, M.; Creutz, C.; Sutin, N. *J. Am. Chem. Soc.* **1977**, *99*, 5615−5623.
(3) Gray, H. B.; Winkler, J. R. *Annu. Rev. Biochem.* **1996**, *65*, 537−561.
(4) Fox, L. S.; Kozik, M.; Winkler, J. R.; Gray, H. B. *Science* **1990**, *247*, 1069−1071.
(5) Closs, G. L.; Miller, J. R. *Science* **1988**, *240*, 440−447.
(6) Nakabayashi, S.; Itoh, K.; Fujishima, A.; Honda, K. *J. Phys. Chem.* **1983**, *87*, 5301−5303.
(7) Lu, H.; Prieskorn, J. N.; Hupp, J. T. *J. Am. Chem. Soc.* **1993**, *115*, 4927−4928.
(8) Lewis, N. S. *J. Phys. Chem. B* **1998**, *102*, 4843−4855.
(9) Lewis, N. S. *Annu. Rev. Phys. Chem.* **1991**, *42*, 543−580.
(10) Fajardo, A. M.; Lewis, N. S. *Science* **1996**, *274*, 969−972.
(11) Fajardo, A. M.; Lewis, N. S. *J. Phys. Chem. B* **1997**, *101*, 11136−11151.
(12) Pomykal, K. E.; Lewis, N. S. *J. Phys. Chem. B* **1997**, *101*, 2476−2484.

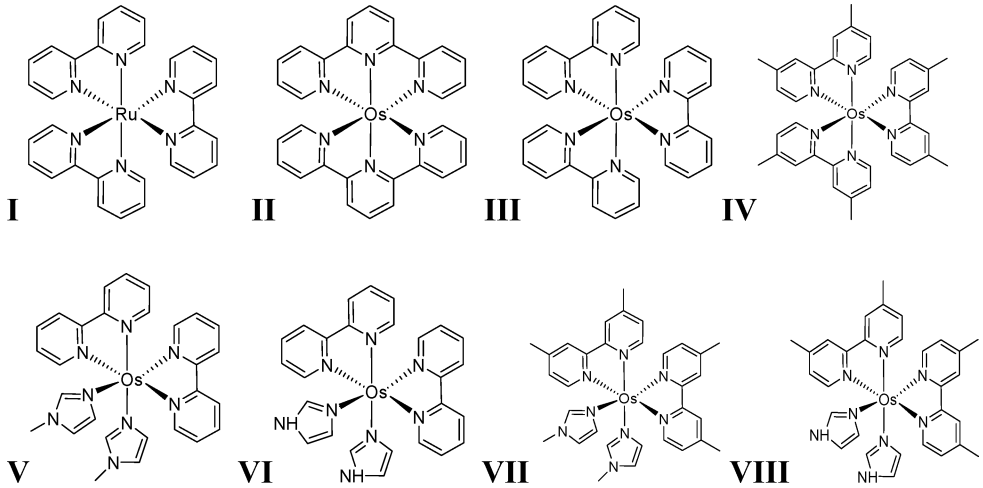

Figure 1. Numerical symbols and chemical names of the redox compounds used in this study, given in the order of decreasing potential. **I** $[Ru(bpy)_3]^{3+/2+}$, **II** $[Os(terpy)_2]^{3+/2+}$, **III** $[Os(bpy)_3]^{3+/2+}$, **IV** $[Os(Me_2bpy)_3]^{3+/2+}$, **V** $[Os(bpy)_2(MeIm)_2]^{3+/2+}$, **VI** $[Os(bpy)_2(Im)_2]^{3+/2+}$, **VII** $[Os(Me_2bpy)_2(MeIm)_2]^{3+/2+}$, **VIII** $[Os(Me_2bpy)_2(Im)_2]^{3+/2+}$.

Several studies using ZnO electrodes in the 1960s noted a linear relationship between the logarithm of the current density, J, and the applied potential, E, with a slope of E versus J of 60 mV/decade, indicating that ZnO/liquid contacts exhibit an "ideal" first-order dependence on the electron concentration at the surface of the semiconductor.[13−16] However, only a few of the redox couples studied, notably $Fe(CN)_6^{3-/4-}$, showed a first-order dependence of the interfacial rate on the concentration of the redox acceptor species in solution. This latter condition is also required to allow a straightforward interpretation of the observed interfacial current density. Another important result of these earlier ZnO studies is that a relatively small frequency dispersion was observed in the differential capacitance measurements, allowing a reliable determination of the surface electron concentration and, additionally, a reliable measurement of the position of the band edges versus a fixed reference electrode. In addition, corrosion or passivation of the surface of the ZnO electrodes was minimal. Subsequent attempts to extract rate constants from steady-state J versus E data were thwarted because most of the simple metal-ion-based redox systems that were investigated, such as Ce^{4+} (in HNO_3 and H_2SO_4), $IrCl_6^{2-}$, V^{3+} (in HCl), and $Ag(NH_3)_2^+$, are known to adsorb onto hydroxylated surfaces or to involve inner-sphere electron-transfer pathways. Little follow-up of these early experiments has apparently occurred over the subsequent four decades.

In this work, the interfacial electron-transfer kinetics of a ZnO semiconductor/liquid interface has been studied at low and high driving forces. To achieve this goal, we have synthesized a series of one-electron outer-sphere redox couples having potentials that span approximately 900 mV (Figure 1) in the band gap region of ZnO. Rate constants have been measured for such systems in contact with n-type ZnO electrodes. NMR line broadening experiments were performed to determine the reorganization energies of the compounds in the same medium as that used to determine the interfacial kinetics at ZnO. Such measurements have allowed a detailed investigation of the dependence of the rate constant for electron transfer on driving force in both the normal and Marcus inverted region, for a homologous series of outer-sphere redox-active compounds at an "ideally" behaving semiconductor/electrode interface.

Scheme 1. Thermodynamic and Kinetics Parameters of a Semiconductor/Liquid Junction[a]

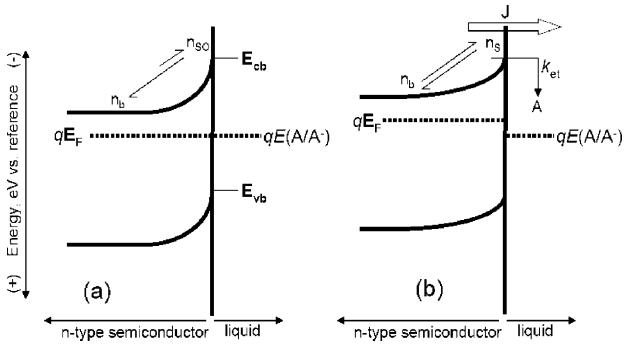

a Energy versus distance for an n-type semiconductor in contact with a redox species (A/A^-). Formation of a space-charge region produces a spatially dependent electric potential drop in the solid. $\mathbf{E}_{cb}$ and $\mathbf{E}_{vb}$ are the energies of the conduction and valence band edges, respectively, and $E(A/A^-)$ is the Nernstian potential of the redox species (A/A^-). The value of $\Delta G^{\circ\prime}$, the standard free-energy change for interfacial charge transfer, is given by $\Delta G^{\circ\prime} = \mathbf{E}_{cb} - qE^{\circ\prime}(A/A^-)$, where $E^{\circ\prime}(A/A^-)$ is the formal reduction potential of the (A/A^-) redox system. The surface and bulk electron concentrations are denoted as n_s and n_b, respectively. (a) At equilibrium, the electrode potential, E, is such that the Fermi level of the semiconductor, $\mathbf{E}_F$, equals $qE(A/A^-)$, and $n_s = n_{so}$, where n_{so} is the surface electron concentration at equilibrium of the solid/liquid interface. (b) If a potential is applied such that the junction is biased away from equilibrium, n_s is not equal to n_{so}, and a nonzero net current, J, flows across the semiconductor/liquid interface.

B. Rate Laws and Models for Charge-Transfer Processes. Scheme 1 depicts the thermodynamic and kinetics parameters that describe electron-transfer processes at a nondegenerately doped n-type semiconductor/liquid interface. No electronic states are present in the band gap region of an ideal semiconductor, so only electrons that are thermally excited to the conduction band for an n-type material can participate in majority carrier based electron-transfer events. At forward bias, the net flux of electrons from the conduction band to randomly dissolved acceptors in solution is given by[17]

$$J(E) = -qk_{et}[A]n_s \qquad (1)$$

where J is the current density (A cm^{-2}); E is the applied

(13) Dewald, J. F. *Bell Technol. J.* **1960**, *39*, 615−639.
(14) Dewald, J. F. *J. Phys. Chem. Solids* **1960**, *14*, 155−161.
(15) Morrison, S. R. *Surf. Sci.* **1969**, *15*, 363−379.
(16) Morrison, S. R.; Freund, T. *J. Chem. Phys.* **1967**, *47*, 1543−1551.

potential (V) relative to a saturated calomel electrode, SCE; q is the charge of an electron (1.6022×10^{-19} C); k_{et} is the electron-transfer rate constant ($cm^4\ s^{-1}$); [A] is the acceptor concentration (cm^{-3}), and n_s is the electron concentration (cm^{-3}) at the surface of the semiconductor. The concentrations of the acceptor, [A], and of the electrons in the conduction band at the surface of the semiconductor, n_s, appear explicitly in the expression for the current density, thus yielding a second-order rate law for the charge-transfer process.

The value of n_s is related to the potential difference between E and the potential of the conduction band edge, $\mathbf{E}_{cb}/q$, through a Boltzmann-type relationship:[8]

$$n_s = N_c e^{(\mathbf{E}_{cb} - qE)/k_B T} \quad (2)$$

where k_B is Boltzmann's constant; T is the temperature; $\mathbf{E}_{cb}$ is the energy of the conduction band edge, and N_c is the effective density of states in the conduction band of the semiconductor. Hence, application of a potential to an ideally behaving semiconductor electrode interface effects a change in the observed current density (i.e., the charge-transfer rate) by changing the value of the electron concentration at the surface of the solid, as opposed to changing the rate constant, or the energetics, of the interfacial charge-transfer process.

If J is shown to follow eq 1, with knowledge of n_s and [A], the value of k_{et} can be calculated from the observed steady-state J versus E data. Unlike the situation for metallic electrodes, the relatively small, and controllable, value of the electron concentration at the semiconductor surface affords the ability to avoid redox-coupled mass-transport limitations on the charge-transfer flux even for reactions at optimal exoergicity. Hence, rate measurements at semiconductor electrodes can be performed using simple steady-state methods with dissolved redox species, even for relatively large values of the interfacial charge-transfer rate constant.

II. Experimental Section

A. Electrodes. Hydrothermally grown, n-type, ⟨0001⟩ oriented, ZnO single crystals having dimensions of approximately $10 \times 10 \times 0.5$ mm were purchased from Commercial Crystal Laboratories, Inc. (Naples, FL). The resistivity of the crystals was reported by the manufacturer to be between 10^1 and $10^4\ \Omega$ cm.

Electrochemical experiments reported in this work were confined to the Zn-rich surface of such electrodes. Due to the limited number of high-quality ZnO single crystals available, a meaningful statistical approach was not feasible. For consistency, all of the data reported herein were collected using a single electrode to evaluate the trends in energetic and kinetics behavior for the entire series of redox couples of interest. At least two other electrodes with nominally identical capacitance versus E behavior to the one reported herein exhibited essentially identical J versus E behavior, for several different contacts, to the electrode reported herein. Other electrodes produced similar trends in the rate constant versus driving force behavior, except that the calculated $-\Delta G^{\circ\prime}$ and k_{et} values for these other electrodes were somewhat smaller for every redox system in the series because these electrodes exhibited more positive flat-band potentials than the electrode reported herein.

The crystal was first polished with water-based diamond suspensions of grain size 6, 3, and 1 μm. The crystal was then chemically polished in a silica/KOH suspension (0.05 μm, pH > 10, South Bay Technology Inc., San Clemente, CA). Ga−In eutectic was used as an ohmic contact, and silver print (GC electronics 22-201, Rockford, IL) was used to connect the Ga−In to a tinned copper wire. White epoxy was used to seal the ZnO electrode assembly in a glass tube. The resulting electrode area was determined by digitizing photographs of a microruler and of the exposed ZnO surface. An area of 0.51 cm^2 was determined with an estimated error of 0.03 cm^2. Before use, the electrode was etched for 7 min in concentrated phosphoric acid (Aldrich), rinsed with 18 MΩ cm resistivity water (Barnstead NANOPure), and blown dry with N_2(g).

B. Electrolyte Solutions. Electrochemical experiments were carried out in a 55 mM phthalate buffer prepared by adding 12 mL of 1.0 M KOH(aq) to 250 mL of 0.11 M potassium hydrogen phthalate (5.76 g) solution, followed by dilution to 500 mL. The pH was then adjusted to pH 4.99 using 1 M KOH(aq). The ionic strength was adjusted to 1.0 M by adding 37.4 g of KCl (Aldrich, 99+%) to provide the supporting electrolyte for the electrochemical measurements.

C. Redox Compounds. Ammonium hexachloroosmate(IV), 2,2′-bipyridine (bpy), 4,4′-dimethyl-2,2′-bipyridine (Me_2bpy), terpyridine (terpy), imidazole (Im), 1-methylimidazole (MeIm), NH_4PF_6, and $(n\text{-}C_4H_9)_4NCl$ (TBACl) were purchased from Aldrich and used as received. All solvents were reagent grade and were used as received. $Ru(bpy)_3Cl_2 \cdot 6H_2O$, **I** (Figure 1), was purchased from Strem Chemicals and used as received. All other compounds were made following modified literature procedures, as described briefly below.[18,19]

1. Synthesis of $[Os(terpy)_2](PF_6)_2$ (II), $[Os(bpy)_3](PF_6)_2$ (III), and $[Os(Me_2bpy)_3](PF_6)_2$ (IV). In a 50 mL round-bottom flask, 3.5 equiv of bpy or Me_2bpy or 2.5 equiv of terpy was added to $(NH_4)_2[OsCl_6]$ (0.25 g, 0.56 mmol) dissolved in 25 mL of ethylene glycol. The solution was heated to reflux for 1 h with rapid stirring under Ar and was then cooled to room temperature. Then, 2−3 equiv of NH_4PF_6(aq) was added, and the resulting PF_6^- salt precipitate of the desired compound was filtered, yielding a dark-green product that was washed with cold water and diethyl ether.

2. Synthesis of $[Os(bpy)_2(MeIm)_2](PF_6)_2$ (V), $[Os(bpy)_2(Im)_2](PF_6)_2$ (VI), $[Os(Me_2bpy)_2(MeIm)_2](PF_6)_2$ (VII), and $[Os(Me_2bpy)_2(Im)_2](PF_6)_2$ (VIII). In a 50 mL round-bottom flask, 2 equiv of bpy or Me_2bpy was added to $(NH_4)_2[OsCl_6]$ (1.1 g, 2.3 mmol) in 30 mL of ethylene glycol. The solution was heated to reflux for 1 h with rapid stirring under Ar and was then cooled to room temperature. To reduce any Os(III) species that may have formed, approximately 100 mL of cold 1 M aqueous $Na_2S_2O_4$ was slowly added, and the solution was cooled for 1 h in an ice bath. The dark precipitate was collected by vacuum filtration, washed with cold water and diethyl ether, and used in further reactions without additional purification.

To make the imidazole complexes, in a 100 mL round-bottom flask, 5−20 equiv of Im or MeIm was then added to the dried product, $[OsCl_2(bpy)_2]$ or $[OsCl_2Me_2bpy_2]$, in 50 mL of ethylene glycol. The solution was heated to reflux for 2−3 h with rapid stirring under Ar and was then cooled to room temperature. Then, 2−3 equiv of NH_4PF_6(aq) was added, and the resulting PF_6^- salt precipitate was filtered, yielding a dark-brown product that was washed with cold water and diethyl ether.

3. Purification and Characterization of the Os Complexes. Metal complexes **II**−**VIII** were purified on an activated neutral alumina column using acetonitrile as the eluent. For **II**−**IV**, a dark-green band was collected, whereas **V**−**VIII** yielded a brown band. The solvent was removed in vacuo. The residue was dissolved in a minimal amount of acetone, and the complex was precipitated by addition of diethyl ether. The product was then filtered and dried under vacuum. Yields in excess of 80% were obtained for **II**−**IV**, and yields were in excess of 30% for **V**−**VIII**. Elemental analysis yielded the following (calculated). **II**: C 37.99 (38.06), H 2.41 (2.56), N 8.89 (8.88). **III**: C

(17) Morrison, S. R. *Electrochemistry at Semiconductor and Oxidized Metal Electrodes*; Plenum: New York, 1980.

(18) Nakabayashi, Y.; Omayu, A.; Yagi, S.; Nakamura, K. *Anal. Sci.* **2001**, *17*, 945−950.

(19) Nakabayashi, Y.; Nakamura, K.; Kawachi, M.; Motoyama, T.; Yamauchi, O. *J. Biol. Inorg. Chem.* **2003**, *8*, 45−52.

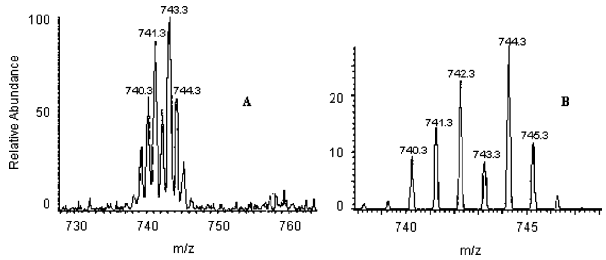

Figure 2. (A) Electrospray mass spectrum of $[Os(Me_2bpy)_3]^{+}$ from $[Os(Me_2bpy)_3]Cl_2$. (B) Simulated isotopic peak distribution for the molecular ion $[OsC_{36}H_{36}N_6]^{+}$.

Table 1. Mass Spectroscopic and Cyclic Voltammetric Results

ion	calcd mass	observed *m/z*	$E^{\circ\prime}$ (V vs SCE)
I	n/a	n/a	1.001
$\mathbf{II}^{2+}$	328	329	0.673
$\mathbf{III}^{2+}$	330	330	0.572
$\mathbf{IV}^{2+}$	372	372	0.385
$\mathbf{V}^{2+}$	333	334	0.248
$\mathbf{VI}^{2+}$	319	320	0.248
$\mathbf{VII}^{2+}$	361	362	0.111
$\mathbf{VIII}^{2+}$	347	348	0.106

[a] Mass peaks of singly charged ions are given for 2^{+} ions that were reduced from the matrix; 1^{+} ions were also observed in all spectra with a m/z 1/2 that of the calculated mass.

37.93 (37.98), H 2.73 (2.55), N 8.64 (8.86). **IV**: C 41.81 (41.86), H 3.49 (3.51), N 7.89 (8.14). **V**: C 35.15 (35.15), H 3.07 (2.95), N 11.34 (11.71). **VI**: C 33.56 (33.63), H 2.46 (2.60), N 11.77 (12.07). **VII**: C 39.22 (37.95), H 3.67 (3.58), N 11.23 (11.06). **VIII**: C 36.65 (36.59), H 3.31 (3.28), N 11.13 (11.37).

Compounds were converted to the chloride salt by dissolving in acetone followed by addition, while stirring, of a concentrated solution of TBACl in acetone. The chloride salt precipitated out of solution, was filtered, washed with acetone and ether, and then dried in vacuo. Elemental analysis yielded the following (calculated). **II**·$2H_2O$: C 47.42 (47.18), H 3.18 (3.17), N 11.12 (11.00). **III**·$4H_2O$: C 45.04 (44.95), H 4.02 (4.02), N 10.48 (10.48). **IV**·$4H_2O$: C 44.57 (48.81), H 4.26 (5.01), N 10.10 (9.49). **V**·$4H_2O$: C 39.63 (41.53), H 3.72 (4.48), N 13.15 (13.84). **VI**·$2H_2O$: C 41.41 (41.88), H 3.66 (3.78), N 14.24 (15.03). **VII**·$2H_2O$: C 47.33 (46.32), H 4.94 (4.86), N 12.20 (13.50). **VIII**·$2H_2O$: C 45.01 (44.94), H 4.48 (4.53), N 12.33 (13.98). Since chloride salts can adsorb water, water was added to the molecular formula to account for the analysis results.

NMR, mass spectroscopic, and cyclic voltammetric data were collected on all of the compounds of interest. Analytic NMR measurements were made on a Varian 300 MHz spectrometer. Spectra were obtained of the PF_6^{-} salts in CD_3CN and of the Cl^{-} salts in D_2O. The expected integration and shifts of the proton peaks of the ligands were observed for both types of salts. NMR spectra of the chloride salts indicated the presence of the expected ligands and the lack of hydrogen-containing impurities, other than water.

Electrospray mass spectroscopic data (Table 1) were collected for compounds **II**−**VIII** and confirmed the composition of the materials. The major peaks were also isotopically resolved and compared to theoretical spectra for the compounds of interest. Figure 2 displays the peaks observed for $[Os(Me_2bpy)_3]^{+}$ along with the theoretically predicted spectrum of this species. The $[Os(Me_2bpy)_3]^{+}$ ion was produced by reduction of $[Os(Me_2bpy)_3]^{2+}$ by the matrix; peaks corresponding to $[Os(Me_2bpy)_3]^{2+}$ were also observed. Differences in mass between the predicted and observed spectra are due to the loss of a hydrogen atom. The agreement between the observed and calculated spectra and isotopic patterns confirmed the composition of each compound.

The formal reduction potential, $E^{\circ\prime}(A/A^{-})$, of each compound (Table 1) was determined using cyclic voltammetry in buffered H_2O with 1 M KCl electrolyte in an ice bath. A graphite disk electrode was used as the working electrode; a platinum mesh was employed as the counter electrode, and an SCE, in a separate cell at room temperature, was used as the reference electrode. Scans were taken from −0.1 to 1.1 V vs SCE at a scan rate of 50−75 mV s^{-1}. An error of ±5 mV was estimated for $E^{\circ\prime}(A/A^{-})$ of each redox couple, as determined from the cyclic voltammetry data.

D. NMR Line Broadening Experiments. NMR spectra were measured on a Varian 500 MHz spectrometer. Since these results were used in the interpretation of electrochemical measurements, the conditions of the two experiments were matched as closely as possible. Measurements were carried out at 3−4 °C in buffered D_2O solutions that contained 1 M KCl. The deuterated buffer was prepared as follows. NaOD in D_2O was added dropwise, until the pH reached 4.50, to a solution of 0.134 g of deutero-phthalic acid dissolved in 10 mL of D_2O (78 mM).

Diamagnetic Os(II) samples of **IV** were prepared by dissolving sufficient **IV**, as the Os(II) chloride salt, to make a 10 mM solution in D_2O that contained 1 M KCl. An aliquot of this solution was oxidized by exposure to Cl_2(g) until the solution turned bright red. To remove dissolved Cl_2(g), the solution was purged with Ar(g), and the resulting sample was used as the pure paramagnetic Os(III) sample of **IV**. Both the diamagnetic and paramagnetic solutions were then diluted by 50% with the buffer solution. Aliquots of the paramagnetic solution were added to the diamagnetic solution, and the resulting solutions were used as mixed samples. Several solutions with different concentrations of paramagnetic species were prepared in this fashion.

Diamagnetic samples of **V** and **VIII** were prepared from the Os(II) chloride salt by making a 5 mM solution in a deuterated buffer (2.5 mM, 1 M KCl). Bulk electrolysis was employed to oxidize controlled amounts of the complex of interest, and aliquots were taken after each bulk electrolysis step. The mass-transport-limited currents recorded with a platinum microelectrode were used to verify the mole fractions of diamagnetic and paramagnetic species of each aliquot. The pure paramagnetic sample was prepared by bulk electrolysis carried out to completion, as verified by the lack of significant anodic faradaic current in the resulting solution.

For data analysis, NMR free-induction decays were imported to Mestrec software and a Fourier transform was performed. Spectra were then exported to Sigma Plot software for analysis. All reported peak positions and line widths were derived from nonlinear least-squares fits of the peak of interest to a Lorentzian line shape. Errors given in the spectral parameters are the standard errors from the peak fitting routine, propagated for the determination of the error in the self-exchange rate constant, k_{se}.

The line-width method[20] was used for proton signals that were not complicated by coupling. Because the osmium polypyridyl compounds of interest in this study are in the fast-exchange regime, the chemical shifts of mixed species were assumed to vary linearly with the mole fraction of species in the solution.[20] Accurate mole fractions, therefore, can be determined by the ratio of the frequency shift to the contact shift[21]

$$X_p = |\nu - \nu_d|/\Delta\nu \qquad (3)$$

where X_p and X_d are the mole fractions of paramagnetic and diamagnetic species, respectively (with $X_d = 1 - X_p$); ν is the frequency shift of a proton peak in the mixed sample; ν_d is the corresponding peak shift in the pure diamagnetic sample, and $\Delta\nu$ is the shift difference between the peaks of the pure paramagnetic and diamagnetic samples ($\Delta\nu = \nu_p - \nu_d$).

E. Electrochemical Measurements. All buffers were deaerated prior to use by purging with Ar, and electrochemical measurements with ZnO were performed under an Ar atmosphere. ZnO electrodes were etched and then immersed in the supporting electrolyte for at least 5

(20) Chan, M. S.; Wahl, A. C. *J. Phys. Chem.* **1978**, *82*, 2542−2549.
(21) Jameson, D. L.; Anand, R. *J. Chem. Educ.* **2000**, *77*, 88−89.

min before being transferred to the electrochemical cell. All experiments were carried out in an ice bath with a solution temperature of ~3 °C. The Os(III) compounds were created in situ via bulk electrolysis using a carbon mesh working electrode to create a 5 mM concentration; a 5% error in [A] was estimated. The concentration of acceptor, [A], was varied by diluting an aliquot of the redox solution with buffer. The Nernstian potential of the solution, $E(\mathrm{A/A^-})$, changed by less than 3 mV during each measurement and by less than 15 mV following dilution. The J versus E data and the open-circuit potential of each electrode were recorded before and after each set of differential capacitance measurements.

Differential capacitance measurements were performed with a Schlumberger Instruments Model 1260 Impedance Gain-Phase Analyzer interfaced to a Model SI1287 potentiostat. Measurement parameters were adjusted to minimize the exposure of the electrode to acidic media, as it is known that ZnO can dissolve in acidic solutions.[22] The differential capacitance versus E behavior of the semiconductor/liquid contact was recorded for DC biases that were stepped in 100 mV increments over the potential range of 0.1−0.8 V vs SCE. A 10 mV AC signal was superimposed on the DC bias. Each capacitance measurement consisted of frequency sweeps from 10^2 to 10^4 Hz in equally spaced logarithmic steps.

To deduce the space-charge capacitance, the impedance spectra were fitted to an equivalent circuit that consisted of the cell resistance, R_s, in series with two parallel components: the resistance to charge transfer, R_{sc}, and the space-charge capacitance, C_{sc}. Because C_{sc} is much less than the differential capacitance, C_{diff}, of either the Helmholtz layer or the double layer, C_{diff} was set equal to C_{sc}.[11,17] A linear regression was used to fit the C_{diff}^{-2} versus E data in accordance with the Mott−Schottky equation:[17]

$$C_{sc}^{-2} = \frac{2}{q\epsilon\epsilon_o N_D A_s^2}\left(E - E_{fb} - \frac{k_B T}{q}\right) \tag{4}$$

where ϵ is the static dielectric constant of the electrode (8.65 for ZnO);[23] ϵ_o is the permittivity of free space; N_D is the dopant density of the semiconductor; A_s is the surface area of the semiconductor electrode, and E_{fb} is the flat-band potential of the semiconductor/liquid contact. Values for N_D and E_{fb} were obtained from the slope and from the x-intercept adjusted by k_BT/q, respectively. With knowledge of N_D and E_{fb}, the energy of the conduction band edge, $\mathbf{E}_{cb}$, was determined using the expression

$$\mathbf{E}_{cb} = qE_{fb} + k_B T \ln\left(\frac{N_D}{N_c}\right) \tag{5}$$

where $N_c = 3.5 \times 10^{18}$ cm^{-3} for ZnO.[24] The interfacial free energy for charge transfer under standard conditions, $\Delta G^{o\prime}$, was then computed for each redox system by subtracting $qE^{o\prime}(\mathrm{A/A^-})$ from $\mathbf{E}_{cb}$.

The J versus E data were obtained with a Schlumberger Instruments Electrochemical Interface Model SI1287 potentiostat. Two scans at a rate of 20 mV s^{-1} were measured. IR corrections were applied to all of the J versus E data, despite the negligible effect due to the low currents in the region of interest. The cell resistance, R_{cell}, was obtained from the fit of the impedance spectra to the equivalent circuit. The data for the low driving force redox couples, **VII** and **VIII**, were also corrected for the concentration overpotential, n_{cone},[25] calculated from the mass-transport-limited cathodic and anodic current densities, $J_{l,c}$ and $J_{l,a}$, respectively, that were measured with a one-sided Pt-foil electrode of known area, according to eqs 6 and 7:

$$\eta_{conc} = \left(\frac{k_B T}{nq}\right)\left\{\ln\left(\frac{J_{l,a}}{-J_{l,c}}\right) - \ln\left(\frac{J_{l,a} - J}{J - J_{l,c}}\right)\right\} \tag{6}$$

$$E_{corr} = E - iR_{cell} - \eta_{conc} \tag{7}$$

with E_{corr} the corrected potential of the semiconductor electrode.

III. Results

A. Measurements of Self-Exchange Rate Constants using NMR Line Broadening. Figure 3 displays the fit of the methyl peak of **IV** to a Lorentzian line shape for a solution of the diamagnetic Os(II) complex and for a solution containing both the Os(II) and Os(III) forms of the complex. The self-exchange rate constant, k_{ex}, was calculated from[20]

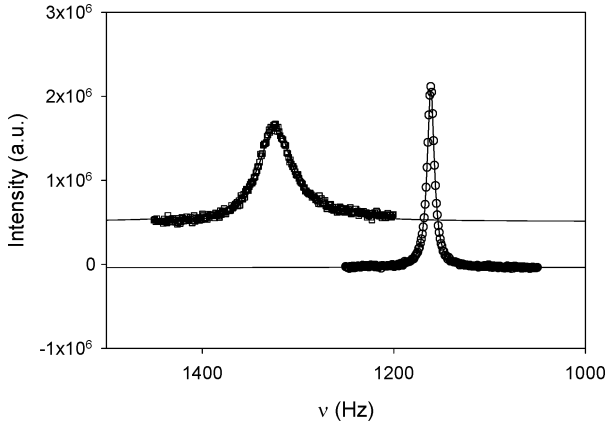

Figure 3. ^{1}H NMR spectra of the methyl proton peak of $Os(Me_2bpy)_3^{2+}$ (circles) and of a mixture of $Os(Me_2bpy)_3^{2+}$ and $Os(Me_2bpy)_3^{3+}$ (squares). The lines indicate the results of nonlinear least-squares fitting of each spectrum.

$$k_{ex} = \frac{4\pi X_d X_p (\Delta\nu)^2}{(W_{dp} - X_d W_d - X_p W_p)C} \tag{8}$$

where W_{dp} is the line width (full width at half-maximum) of the mixed species resonance peak; W_p and W_d are the line widths of the paramagnetic and diamagnetic peaks, respectively, and C is the total concentration of exchanging species. The line width of the diamagnetic species was ~3−5 Hz. The reported values of k_{se} are averages of measurements on at least three compositionally different mixed samples. A value of k_{se} was also determined from the line broadening of the methyl and of the 3,3′ proton peak, as both are uncoupled. This analysis produced a value of $k_{se} = 1.1 \times 10^8$ M^{-1} s^{-1} (Table 2) for **IV** in buffered D_2O (pH = 4.5) at 3 °C and 1 M ionic strength.

Table 2. Relevant Parameters, Self-Exchange Rate Constants, and Reorganization Energies from ^{1}H NMR Line-Broadening Measurements in Buffered D_2O (pH = 4.5) with an Ionic Strength of 1 M at 3 °C

	ν_d[a] (Hz)	$\Delta\nu$[b] (Hz)	W_p[c] (Hz)	$k_{se} \times 10^{-7}$ (M^{-1} s^{-1})	λ_{se} (eV)
$\mathbf{IV_{Me}}$[d]	1161	8297	194	11.3 ± 0.7	0.64 ± 0.01
$\mathbf{IV_{3,3'}}$[d]	4064	4892	155	12 ± 3	0.64 ± 0.02
V	1643	5079	101	7.3 ± 0.8	0.68 ± 0.01
VIII	1122	3857	141	7.1 ± 0.7	0.69 ± 0.01

[a] Quantity ν_d is the shift of the pure diamagnetic species. [b] $\Delta\nu$ is the shift difference between the diamagnetic and paramagnetic species. [c] W_p is the paramagnetic line width. [d] Subscripts Me and 3,3′ designate results from the methyl protons and 3,3′ protons, respectively, for compound **IV**.

(22) Gerischer, H.; Sorg, N. *Electrochim. Acta* **1992**, *37*, 827−835.
(23) Bhargava, R. *Properties of Wide Bandgap II−VI Semiconductors*; Inspec: London, 1997; Series No. 17.
(24) Sze, S. M. *The Physics of Semiconductor Devices*, 2nd ed.; Wiley: New York, 1981.
(25) Bard, A. J.; Faulkner, L. R. *Electrochemical Methods: Fundamentals and Applications*; John Wiley & Sons: New York, 2001.

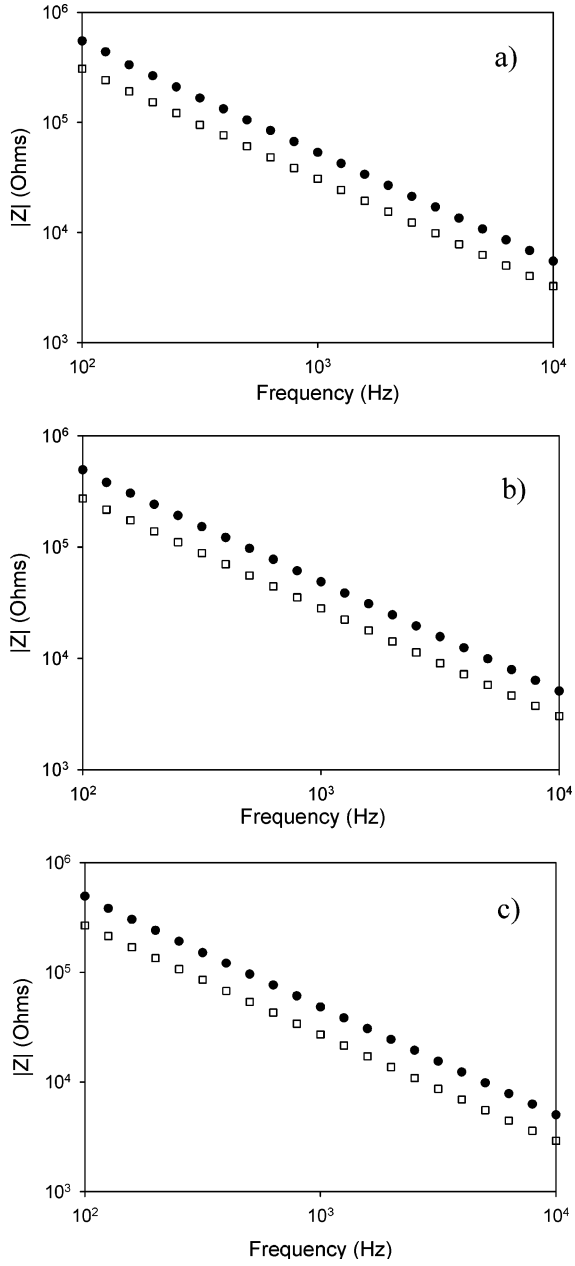

Figure 4. Bode plots of the magnitude of the impedance versus frequency for **I** (a), **II** (b), and **VII** (c) biased at 0.8 V vs SCE (solid circles) and 0.2 V vs SCE (open square).

Self-exchange rate constants were also determined for compounds **V** and **VIII**. Both of these compounds have uncoupled methyl protons, facilitating a straightforward analysis of the NMR data. Values of k_{se} were calculated to be 7×10^7 M^{-1} s^{-1} for **V** and **VIII** (Table 2).

B. Electrochemical Data. 1. Differential Capacitance versus Applied Potential Measurements. Figure 4 presents representative Bode plots for some of the semiconductor/liquid junctions studied in this work. Data are shown for two applied potentials, 0.8 and 0.2 V vs SCE. The Bode plots of the impedance magnitude, |Z|, were linear over at least 2 orders of magnitude variation in ac signal frequency, *f*, having slopes of about −1 and phase angles of the current versus ac voltage of about −90°. The observed impedance of these systems was thus dominated by a single capacitive circuit element, with $Z_{im} \approx (2\pi f C_{diff})^{-1}$.[11]

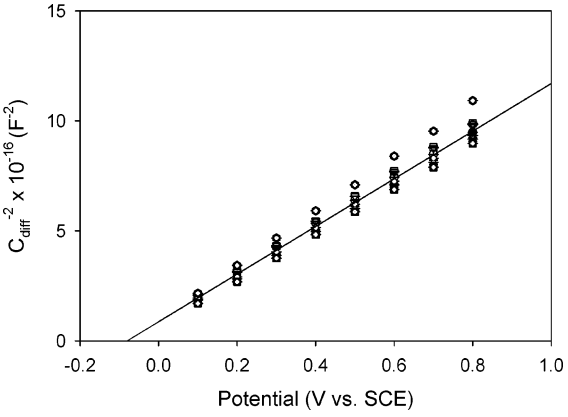

Figure 5. Mott−Schottky plots of compounds **I** (hexagon w/cross), **II** (open circle), **III** (open square), **IV** (open triangle up), **V** (open triangle down), **VI** (open diamond), **VII** (triangle w/cross up), and **VIII** (square w/cross). The line indicates the least-squares fit of all of the data.

To obtain values for C_{sc}, which is taken to be equal to C_{diff}, the impedance spectra were fitted over the frequency range of 10^2-10^4 Hz to the equivalent circuit described above. No frequency dependence of the capacitance was observed, resulting in very small errors (<1%) for each fit. The series resistance of the system, R_s, was essentially constant for all measurements, with a value of 850 Ω. This series resistance can be accounted for by the ohmic resistance of the sample because the measured impedance of other electrodes prepared from crystals from the same batch was ∼1 kΩ.

Figure 5 displays Mott−Schottky plots in the form of C_{diff}^{-2} versus E data for all contacts grouped and weighted by their respective (negligible) errors. All of the plots were linear, as predicted by eq 4. The resulting slope and intercept of a linear least-squares fit were used to extract values for N_d and E_{fb}, respectively. The standard errors resulting from the fit were used to calculate the errors in N_d and E_{fb}, producing values of $E_{fb} = -0.10 \pm 0.01$ V vs SCE and $N_d = (5.8 \pm 0.6) \times 10^{14}$ cm^{-3}. Equation 5 was then used to calculate a value for $\mathbf{E}_{cb}/q = -0.31 \pm 0.01$ V vs SCE. The invariance of the capacitance data at a fixed electrode potential for all of the compounds, despite the large variation in the Nernstian potential of the cells, confirms that the band-edge position is invariant (the "ideal" model) rather than changing with the solution potential (the Fermi level pinning situation).

C_{diff}^{-2} versus E measurements were also performed in solutions that had varying concentrations of oxidized and reduced species of the same redox couple. For all of the junctions studied, the band-edge positions remained constant, to within 15 mV, after a 10-fold reduction in acceptor concentration.

2. Current Density versus Applied Potential Measurements. All of the junctions showed rectifying behavior, producing a limiting anodic current density and an exponentially increasing cathodic current density, in accord with the diode equation:

$$J = -J_0(e^{-qE_{corr}/\gamma k_B T} - 1) \qquad (9)$$

where J_0 is the exchange current density, γ is the diode quality factor, and E_{corr} is the applied potential corrected for both concentration overpotential and for series resistance losses in the electrochemical cell (eq 7).

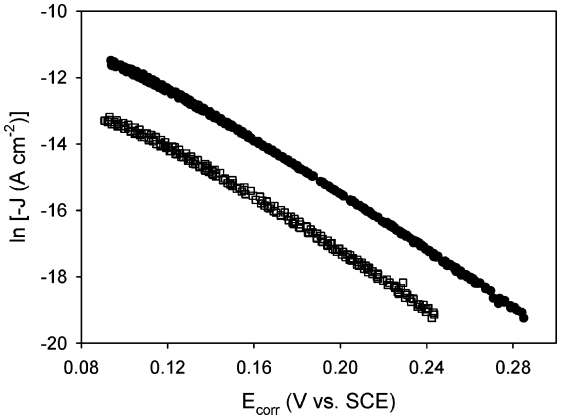

Figure 6. Plots of the dark current density versus E_{corr} for compound **III** at high concentration ([A] = 5 mM; filled circles) and low concentration ([A] ≈ 0.5 mM; open squares). As noted in the text, a decrease in [A] should result in a shift of the $J-E_{corr}$ curve according to $(k_BT/q)\ln([A]_{high}/[A]_{low})$. Potentials are referenced to SCE.

Table 3. Results of Current Density versus Applied Potential Measurements, Barrier Height, and Rate Constant Determinations

compound	γ_{high}[a]	γ_{low}[a]	ΔE (theor)[b] (mV)	$qE(A/A^-) - E_{cb}$[c] (eV)	k_{et}[d] ($cm^4\ s^{-1}$)
I	1.33	1.53	55 (60)	1.30 ± 0.01	$(1.4 \pm 0.6) \times 10^{-19}$
II	1.05	1.15	44 (54)	0.96 ± 0.01	$(2 \pm 1) \times 10^{-17}$
III	1.03	1.02	42 (51)	0.86 ± 0.01	$(1.6 \pm 0.7) \times 10^{-16}$
IV	1.04	1.06	50 (54)	0.67 ± 0.01	$(6 \pm 2) \times 10^{-17}$
V	1.06	1.14	46 (48)	0.54 ± 0.01	$(2 \pm 1) \times 10^{-17}$
VI	1.02	1.19	35 (45)	0.54 ± 0.01	$(3 \pm 1) \times 10^{-17}$
VII	1.06	1.19	50 (54)	0.40 ± 0.01	$(5 \pm 2) \times 10^{-18}$
VIII	1.19	1.29	25 (34)	0.40 ± 0.01	$(6 \pm 2) \times 10^{-18}$

[a] The quantities γ_{high} and γ_{low} are the diode quality factors at high acceptor concentration, $[A]_{high}$, and low acceptor concentration, $[A]_{low}$, respectively. The value of $[A]_{high}$ was always 5.0 mM, and $[A]_{low} \approx 0.5$ mM. [b] The theoretical shift of the J versus E_{corr} data was calculated by $\Delta E(\text{theor}) = (k_BT/q)\ln(J_{l,c,high}/J_{l,c,low})$. [c] The quantity $qE(A/A^-) - E_{cb}$ was calculated using the high acceptor concentration data. [d] As noted in the text, k_{et} was calculated using the high acceptor concentration data for all redox systems investigated.

Figure 6 displays plots of $\ln(-J)$ versus E_{corr} for compound **III** (plots for all other compounds investigated in this work are given as Supporting Information). The diode quality factors were close to 1.0, in accord with expectations for a process that is kinetically first-order in the concentration of electrons at the surface of the semiconductor. The dependence of the rate on the concentration of acceptor species in the solution was determined by reducing [A], which produced shifts of the J versus E_{corr} data, $\Delta E = (k_BT/q)\ln([A]_{high}/[A]_{low})$, as expected for a first-order process in [A]. The magnitude of the change in [A] was verified by measuring the limiting cathodic current densities at both acceptor concentrations, $J_{l,c,high}$ and $J_{l,c,low}$, with a Pt microelectrode, and the theoretical shift of the J versus E_{corr} data was calculated by $\Delta E(\text{theor}) = (k_BT/q)\ln(J_{l,c,high}/J_{l,c,low})$. Values of γ, ΔE, and ΔE(theor) are given in Table 3 for the systems of interest in this work.

3. Rate Constants for Interfacial Charge Transfer, k_{et}. Since nondegenerately doped semiconductor electrodes have relatively little Frumkin correction associated with the liquid part of the solid/liquid double layer,[8] the acceptor concentration can be assumed to be equal to the bulk value. The surface electron concentration at each applied potential, $n_s(E)$, was computed according to eq 2 using the conduction band-edge energy extracted from the flat-band potential determinations (eq 5). The value of k_{et} was then readily calculated in accordance with the rate law given in eq 1, by dividing J by the quantity $\{-qn_s[A]\}$ at a given potential. The J versus E data collected at the largest acceptor concentration were used to minimize the error in the concentration and because the diode quality factors were close to 1 (typically $1 < \gamma < 1.1$) under such conditions. The quoted k_{et} for each contact represents the average of values calculated using the same high cathodic current density portion of the J versus E curve ($-(1-2) \times 10^{-6}$ A cm^{-2}) for each redox couple. A standard error analysis was performed in conjunction with calculation of the rate constants by propagating the errors of all measured parameters used in the calculation of k_{et}. The error in $\mathbf{E}_{cb}$ dominated the error in k_{et}, due to the exponential dependence of n_s on ($\mathbf{E}_{cb} - qE$). Table 3 summarizes the values of k_{et} determined for each of the ZnO/H_2O−redox couple junctions evaluated in this study.

IV. Discussion

A. Reorganization Energies. Self-exchange rate constants of $k_{se} = 2 \times 10^7$ M^{-1} s^{-1} for **III** and **IV** and $k_{se} = 1 \times 10^7$ M^{-1} s^{-1} for **I** have been measured in CH_3CN at 31 °C with PF_6^- as the counterion and at an ionic strength of ~0.1 M.[20] Rate constants were found to be larger in water and to increase with ionic strength, with a value of $k_{se} \approx 2 \times 10^9$ M^{-1} s^{-1} estimated for the ClO_4^- salt of **I** at 25 °C in a 1 M $HClO_4$ solution.[26] Comparison of these results highlights the effects that solvent, counterion, and ionic strength have on k_{se}. Thus, in our study, the self-exchange rate constants were measured under conditions (buffered D_2O with Cl^- counterion and 1 M KCl at 3 °C) that were as close as possible to those used in the electrochemical measurements on ZnO.

The self-exchange rate constants for the redox couples employed were all very similar. A mean value of $(8.6 \pm 0.7) \times 10^7$ M^{-1} s^{-1} (D_2O, 1 M KCl, 3 °C) was measured here for complexes **IV**, **V**, and **VIII**. The self-exchange rate constants of a series of osmium tetramethyl, dimethyl, and unsubstituted phenanthroline complexes have been previously observed to vary only by a factor of 2.[27] Therefore k_{se} is assumed to be similar for **I**, **III**, and **IV** under our conditions. In addition, k_{se} for **II** is also assumed to be similar to that for **III**−**IV** since **II** has the same metal center and very similar ligands. The rate constants for **V** and **VIII** were taken to be representative of values for compounds **V**−**VIII**. No diffusion corrections were made to the measured self-exchange rate constants since the values are significantly below the diffusion-limited value of ~3×10^9 M^{-1} s^{-1}.[28]

The reorganization energy, λ_{se}, for a given species in a self-exchange electron-transfer process can be related to the self-exchange rate constant by the expression[1,28−31]

$$k_{ex} = K_A\kappa_{el}\nu_n\Gamma e^{-\lambda_{se}/4k_BT} \qquad (10)$$

where K_A is the equilibrium constant for the formation of the

(26) Young, R. C.; Keene, F. R.; Meyer, T. J. *J. Am. Chem. Soc.* **1977**, *99*, 2468−2473.
(27) Triegaardt, D. M.; Wahl, A. C. *J. Phys. Chem.* **1986**, *90*, 1957−1963.
(28) Sutin, N. *Acc. Chem. Res.* **1982**, *15*, 275−282.
(29) Meyer, T. J.; Taube, H. In *Comprehensive Coordination Chemistry*; Wilkinson, S. G., Gilliard, R. D., McCleverty, J. A., Eds.; Pergamon Press: New York, 1987; Vol. 1, p 331.
(30) Sutin, N. *Prog. Inorg. Chem.* **1983**, *30*, 441−498.
(31) Brunschwig, B. S.; Logan, J.; Newton, M. D.; Sutin, N. *J. Am. Chem. Soc.* **1980**, *102*, 5798−5809.

precursor complex of the reactants; κ_{el} is the electronic transmission coefficient; ν_n is the effective nuclear vibration frequency of the activated complex, and Γ is a correction for nuclear tunneling. For an ionic strength of 1 M, the work to bring two positively charged species together is less than k_BT, which implies that $K_A \approx 1$.[32,33] Given the similarity of the complexes studied, they are assumed to have similar values of $\kappa_{el} \approx 1$ (i.e., the reactions are adiabatic).[31]

The total reorganization energy in self-exchange reactions is comprised of changes in the bond lengths and angles in the inner coordination sphere of the complexes, $\lambda_{se,in}$, and changes in the polarization of the solvent in the outer coordination sphere, $\lambda_{se,out}$ ($\lambda_{se} = \lambda_{se,in} + \lambda_{se,out}$). For Os and Ru complexes that involve bipyridyl ligands, the inner-sphere does not undergo significant changes upon electron transfer.[34] The reorganization energy is, therefore, dominated by the solvent reorganization energy which has a significant effect on ν_n.[31] For these reactions, ν_n was taken to be 10^{11} s^{-1}.[29,35] The values of λ_{se} obtained using eq 9 with the measured values of k_{se} are 0.67 ± 0.04 eV (Table 2).

The outer-sphere reorganization energy for two identical spherical reactants in solution can be calculated as[1]

$$\lambda_{out} = \frac{(\Delta zq)^2}{4\pi\epsilon_0}\left[\left(\frac{1}{a} - \frac{1}{R}\right)\left(\frac{1}{n^2} - \frac{1}{\epsilon}\right)\right] \qquad (11)$$

where Δz is the change in charge of each reactant species to form products, a is the radius of the reactant; R is the reactant center-to-center separation; n is the refractive index of the solvent (1.3438 for 0.98 M KCl in H_2O at 20 °C, with a very small temperature dependence[36]), and ϵ is the static dielectric constant of the solvent (86.5 for H_2O at 3 °C[36]). Using a = 0.60 nm and R = 1.2 nm produces a value of $\lambda_{se,out}$ = 0.65 eV, in excellent agreement with the value derived from the self-exchange rate-constant measurements (Table 2).

B. Differential Capacitance versus Applied Potential Measurements. The nearly ideal behavior of the Mott−Schottky plots allowed accurate determination of the flat-band potentials for the ZnO/H_2O interfaces of interest. The E_{fb} values for a given ZnO/liquid contact did not vary significantly as the measurement frequency was changed. Furthermore, E_{fb} values were essentially constant vs SCE as the Nernstian potential of the cell was changed by ∼0.9 V by varying the redox species in the homologous series of compounds investigated in this work (Figure 5).

In prior work on ZnO, the pH dependence of E_{fb} was studied and the predicted $2.3k_BT/q$ shift of E_{fb} per pH unit was verified.[37] A value for $E_{fb} \approx -0.26$ V vs SCE was determined at 25 °C at pH 5 with $N_d = 5 \times 10^{16}$ cm^{-3}, which corresponds to a value of $\mathbf{E}_{cb}/q \approx -0.37$ V vs SCE. In another report, a value for E_{fb} of −0.33 V vs SCE was found for $N_d = 7 \times 10^{14}$ cm^{-3} at 25 °C at pH 8.5,[14] which corresponds to a value of $\mathbf{E}_{cb}/q \approx -0.34$ V vs SCE at pH 5. Our experimental value of $\mathbf{E}_{cb}/q = -0.31 \pm 0.01$ V vs SCE (calculated using eq 5 with $E_{fb} = -0.10 \pm 0.01$ V vs SCE, $N_d = (5.8 \pm 0.6) \times 10^{14}$ cm^{-3}, and T = 276 K) at pH 5 is therefore in good agreement with prior results on ZnO in H_2O.

C. Current Density versus Applied Potential Measurements. A notable feature of the ZnO/H_2O contacts reported herein is their nearly ideal J versus E behavior.[11] Diode quality factors for data collected at high acceptor concentrations were generally found to be between 1 and 1.1, and the J versus E curves shifted by the theoretically expected amounts as the acceptor concentration was varied. These observations imply that the interfacial kinetics follows the rate law of eq 1 and indicate that surface-state effects do not dominate the charge-transfer processes of the systems investigated.[11]

D. Dependence of Interfacial Charge-Transfer Rate Constants on Driving Force: Comparison between Theory and Experiment. One of the most interesting predictions of Marcus theory is that of the inverted region, in which the electron-transfer rate constant decreases with increasing driving force. The maximal rate for a molecular donor−acceptor system is observed when the standard free-energy change for the reaction, $\Delta G^{\circ\prime}$, exactly cancels the reorganization energy, λ. When the driving force is either increased or decreased relative to this point, an energy barrier is present for the reaction, and the rate decreases.[4,5,38−40]

The Marcus description of electron transfer has been generalized for interfacial electron-transfer reactions for both metal and semiconductor electrodes.[17] Metal electrodes, in contrast with molecules, have many closely spaced electronic levels. The rate of electron transfer from a metal electrode to a redox molecule in solution consists of a summation of rates from each of the occupied metal levels, with each level having a rate that is characterized by the Marcus free-energy relationship. Thus, when the driving force for the reaction is made high enough (the electrode potential is made negative enough), an inverted region barrier and a decreased rate of electron transfer will be produced from the highest occupied energy levels. Since there are many closely spaced levels of lower energy, however, there will always be occupied electronic states at optimal exoergicity that dominate the interfacial current. Thus, for metal electrodes, the total rate will not decrease with driving force, which precludes the direct observation of the inverted region.

An ideal semiconductor has no electronic levels in the band gap region, so only electrons with energies near the conduction band, for an n-type material, can contribute to the current flow. This situation is then analogous to a donor−acceptor system. Thus, as the driving force of the reaction increases, the electron-transfer rate of the conduction band electrons should increase, reach a maximal value, and then decrease. It should, therefore, be possible to observe directly the inverted region for semiconductor/liquid contacts.

Several different levels of theory have been used to derive an expression for the rate constant at optimal exoergicity of an interfacial electron transfer for a semiconductor electrode in contact with an acceptor species in solution. These approaches include a simple collisional model[8−11,41] and an electronic coupling model based on Marcus' treatment of electron transfer

(32) Sutin, N.; Brunschwig, B. S. ACS Symposium Series 198, 1982, 105−135.
(33) Sutin, N. In *Tunneling in Biological Systems*; Chance, B., Marcus, R., DeVault, D. C., Schrieffer, J. R., Frauenfelder, H., Sutin, N., Eds.; Academic Press: New York, 1979; pp 201−228.
(34) Biner, M.; Burgi, H.-B.; Ludi, A.; Rohr, C. *J. Am. Chem. Soc.* **1992**, *114*, 5197−5203.
(35) Marcus, R. A. *J. Phys. Chem.* **1963**, *67*, 853−857.
(36) Lide, D. R. *CRC Handbook of Chemistry and Physics*, 81st ed.; CRC Press: Boca Raton, FL, 2001.
(37) Lohmann, F. *Ber. Bunsen-Ges. Phys. Chem.* **1966**, *70*, 428−434.
(38) McCleskey, T. M.; Winkler, J. R.; Gray, H. B. *Inorg. Chim. Acta* **1994**, *225*, 319−322.
(39) Creutz, C.; Sutin, N. *J. Am. Chem. Soc.* **1977**, *99*, 241−243.
(40) Closs, G. L.; Calcaterra, L. T.; Green, N. J.; Penfield, K. W.; Miller, J. R. *J. Phys. Chem.* **1986**, *90*, 3673−3683.
(41) Gerischer, H. *J. Phys. Chem.* **1991**, *95*, 1356−1359.

at the interface of two immiscible liquids.[42−44] An electronic coupling model based on the Fermi Golden Rule applied to the case of a semiconductor electrode in contact with a random distribution of acceptor species in solution has produced the following expression for the rate constant:[45]

$$k_{et} = \frac{2\pi}{\hbar} \frac{1}{(4\pi k_B T \lambda_{sc})^{1/2}} \left\{\overline{H^2_{AB,sc}}\right\} \left\{\beta_{sc}^{-1}\right\} \left\{\frac{l_{sc}}{d_{sc}^{2/3}(6/\pi)^{1/3}}\right\} \left[\exp\left\{\frac{-[(\overbrace{E_{CB} - qE^{o\prime}}^{\Delta G^{o\prime}}) + \lambda_{sc}]^2}{(4k_B T \lambda_{sc})}\right\}\right] \quad (12)$$

where β_{sc} is the coupling attenuation factor; l_{sc} is the effective coupling length in the semiconductor; λ_{sc} is the reorganization energy of the acceptor species near the semiconductor electrode, and d_{sc} is the atomic density of the solid. The quantity $\overline{H^2_{AB,sc}}$ represents the square of the matrix element that couples reactant and product states at energy **E**, averaged over all degenerate states in the semiconductor in a plane parallel to the electrode surface. This value is assumed to be independent of energy over the range of interest.[45] The subscript "sc" indicates parameters for a semiconductor electrode. Equation 12 can be rewritten as

$$k_{et} = k_{et,max} \exp\left\{\frac{-(\Delta G^{o\prime} + \lambda_{sc})^2}{4\lambda_{sc} k_B T}\right\} \quad (13)$$

where the prefactor has been combined into $k_{et,max}$, which is the rate constant at optimal exoergicity. While $k_{et,max}$ is not independent of the reorganization energy, and thus will vary for different redox couples, this variation is modest.

The similarity in the values of the self-exchange rate constants for the complexes studied indicates that both the electronic coupling in homogeneous solution and the reorganization energies are essentially constant. For the electrode reactions, since all compounds are coupling to the same electrode, the electronic coupling coefficient, H_{AB}, is also likely to be similar for the redox species of concern.

Figure 7 shows a semilogarithmic plot of k_{et} versus the standard driving force for interfacial electron transfer, $-\Delta G^{o\prime} = qE^{o\prime}(A/A^-) - \mathbf{E}_{cb}$. The rate constant at optimal exoergicity, $k_{et,max}$, is obtained when $\Delta G^{o\prime} = -\lambda_{sc}$, and has a value of $\sim 10^{-16}$ cm^4 s^{-1}.[45] A k_{et} versus $\Delta G^{o\prime}$ curve calculated according to eq 13 with $k_{et,max} = 10^{-16}$ cm^4 s^{-1} and $\lambda_{sc} = 0.67$ eV (the value derived from self-exchange measurements; see discussion of the reorganization energy below) has been superimposed on the plot of Figure 7a (solid line). The agreement between the experimental data and theory is very good.

An uncertainty in the absolute value of E_{fb} would introduce a constant offset in the standard driving force, and resulting rate constants for all compounds, but such an error in E_{fb} and/or N_d would not change the observed trend of the rate constant with increasing driving force. The interfacial rate constant for **I** was observed to be 2 orders of magnitude smaller than that for **II**, despite >300 mV greater driving force. Although complex **I** has a metal center different than those of complexes **II**−**VIII**, the self-exchange rate constants have been shown to be very similar for analogous Os and Ru polypyridyl complexes.[20] These results, therefore, support the theoretical expectation of the Marcus inverted region for these interfacial electron-transfer processes.

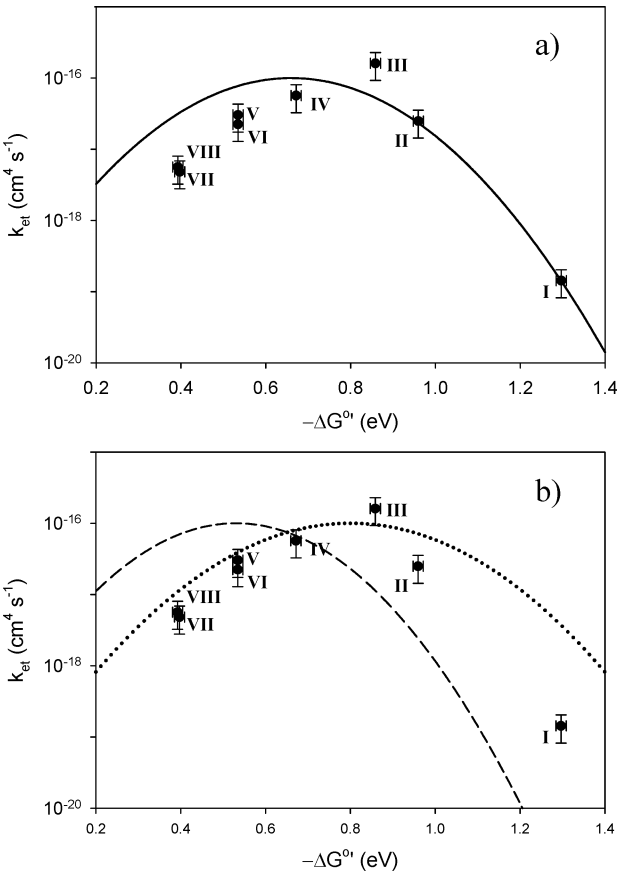

Figure 7. Plots of the electron-transfer rate constant for compounds **I**−**VIII** as a function of the standard driving force, $-\Delta G^{o\prime} = qE^{o\prime}(A/A^-) - \mathbf{E}_{cb}$, for the redox systems investigated. (a) The solid line represents the predicted k_{et} versus $\Delta G^{o\prime}$ behavior for $k_{et,max} = 1 \times 10^{-16}$ cm^4 s^{-1} and $\lambda_{sc} = 0.67$ eV. (b) The dotted line represents the predicted k_{et} versus $\Delta G^{o\prime}$ behavior for $k_{et,max} = 1 \times 10^{-16}$ cm^4 s^{-1} and $\lambda_{sc} = 0.8$ eV, and the dashed line is the predicted k_{et} versus $\Delta G^{o\prime}$ behavior for $k_{et,max} = 1 \times 10^{-16}$ cm^4 s^{-1} and $\lambda_{sc} = 0.53$ eV.

The value of the reorganization energy for an electron-transfer reaction between a redox couple and a ZnO electrode, where both the redox couple in solution and the image charge in the semiconductor contribute to the total reorganization energy, is expected to be less than that for the self-exchange reaction of the couple in homogeneous solution. A theoretical value for the outer-sphere reorganization energy, $\lambda_{sc,out}$, of a redox couple at a ZnO electrode can be calculated by eq 14:[46,47]

$$\lambda_{sc,out} = \frac{(\Delta z q)^2}{8\pi\varepsilon_0}\left[\frac{1}{a}\left(\frac{1}{n_{Sol}^2} - \frac{1}{\varepsilon_{Sol}}\right) - \frac{1}{2R_e}\left(\left(\frac{n_{ZnO}^2 - n_{Sol}^2}{n_{ZnO}^2 + n_{Sol}^2}\right)\frac{1}{n_{Sol}^2} - \left(\frac{\varepsilon_{ZnO} - \varepsilon_{Sol}}{\varepsilon_{ZnO} + \varepsilon_{Sol}}\right)\frac{1}{\varepsilon_{Sol}}\right)\right] \quad (14)$$

where n_{ZnO} and n_{Sol} are the refractive index of ZnO (1.9[23,48]) and the aqueous solution, respectively; ϵ_{ZnO} and ϵ_{Sol} are the static dielectric constants of ZnO (8.65[23]) and the solution, respectively, and R_e is the distance from the acceptor to the electrode.

(42) Marcus, R. A. *J. Phys. Chem.* **1990**, *94*, 1050−1055.
(43) Pomykal, K. E.; Fajardo, A. M.; Lewis, N. S. *J. Phys. Chem.* **1996**, *100*, 3652−3664.
(44) Gao, Y. Q.; Georgievskii, Y.; Marcus, R. A. *J. Chem. Phys.* **2000**, *112*, 3358−3369.
(45) Royea, W. J.; Fajardo, A. M.; Lewis, N. S. *J. Phys. Chem. B* **1997**, *101*, 11152−11159.
(46) Kuciauskas, D.; Freund, M. S.; Gray, H. B.; Winkler, J. R.; Lewis, N. S. *J. Phys. Chem. B* **2001**, *105*, 392−403.
(47) Marcus, R. A. *J. Phys. Chem.* **1991**, *95*, 2010−2013.
(48) Ashkenov, N.; Mbenkum, B. N.; Bundesmann, C.; Riede, V.; Lorenz, M.; Spemann, D.; Kaidashev, E. M.; Kasic, A.; Schubert, M.; Grundmann, M.; Wagner, G.; Neumann, H.; Darakchieva, V.; Arwin, H.; Monemar, B. *J. Appl. Phys.* **2003**, *93*, 126−133.

Using $a = 0.60$ nm and $R_e = 0.60$ nm produces a value of $\lambda_{sc,out} = 0.53$ eV, which is approximately 80% of the outer-sphere reorganization energy of this system in a self-exchange reaction.

A k_{et} versus $\Delta G^{\circ\prime}$ curve calculated according to eq 13 with $k_{et,max} = 10^{-16}$ cm^4 s^{-1} and $\lambda_{sc,out} = 0.53$ eV is superimposed on the plot of Figure 7b (dashed line). Such a curve yields a poor fit to the experimental data, with a λ_{sc} that is too low. Inspection of the plot indicates that the maximum rate constant occurs at $-\Delta G^{\circ\prime} \approx 0.8$ eV, which implies a λ_{sc} for our series of ~0.8 eV. A k_{et} versus $\Delta G^{\circ\prime}$ curve calculated according to eq 13 with $k_{et,max} = 10^{-16}$ cm^4 s^{-1} and $\lambda_{sc} = 0.8$ eV is superimposed on the plot of Figure 7b (dotted line). This theoretical curve fits the low driving force regime well; however, it deviates significantly for the high driving force compounds. The reorganization energy derived from the self-exchange reactions, and calculated according to eq 11, appears to be the best estimate for the reorganization energy of the redox compounds investigated herein at the ZnO/water interface. The slight increase in reorganization energy over that calculated from eq 14 may indicate some contribution to the reorganization energy arising from the electrode and is consistent with similar observations for interfacial charge-transfer processes of silicon electrodes, as reported previously.[10,11] However, clearly most of the reorganization energy for ZnO/redox systems investigated is well described by expectations based on eq 14.

V. Conclusions

The ZnO/H_2O junctions displayed nearly ideal energetic and kinetics behavior in contact with a homologous series of osmium polypyridyl redox couples. Differential capacitance measurements showed that the band edges of ZnO were fixed to within 10 mV with respect to SCE when the solution potential was changed by ~900 mV. Current density versus potential measurements displayed a first-order dependence on acceptor and surface electron concentrations. This behavior allowed the experimental determination of interfacial electron-transfer rate constants for such systems. The driving force was changed by varying the formal reduction potential of the redox couple in solution. The reaction with the highest driving force had the smallest rate constant. This observation of decreasing rate constant with increasing driving force indicates that semiconductor/liquid contacts can operate in the inverted regime with nonadsorbed outer-sphere redox systems.

Acknowledgment. We acknowledge the Department of Energy, Office of Basic Energy Sciences, for support of this work. Dr. Mona Shahgholi provided helpful assistance in acquiring mass spectroscopic data, and Drs. Nagarajan Srivatsan and Norman Sutin are acknowledged for helpful conversations.

Supporting Information Available: Additional plots of dark current density versus E_{corr} for compounds **I**, **II**, and **IV**−**VIII**. This material is available free of charge via the Internet at http://pubs.acs.org.

JA0436188